IEEE Access
Multidisciplinary | Rapid Review | Open Access Journal

Received August 23, 2020, accepted September 6, 2020, date of publication September 11, 2020,
date of current version September 24, 2020.

Digital Object Identifier 10.1109/ACCESS.2020.3023626

Distributed Fiber Optic Sensing and Data Processing of Axial Loaded Precast Piles

YIJIE SUN[1,2], XUAN LI[1], CUN REN[1], HONGZHONG XU[1], AND AIMIN HAN[1]
[1]College of Transportation Science and Engineering, Nanjing Tech University, Nanjing 210009, China
[2]Ministry of Water Resources Center for Levee Safety and Disease Prevention Research, Zhengzhou 450003, China

Corresponding author: Hongzhong Xu (hzhxu@njtech.edu.cn)

This work was supported in part by the National Natural Science Foundation of China under Grant 41877244 and Grant 41702315, and in part by the Ministry of Water Resources Center for Levee Safety and Disease Prevention Research Open Project Fund under Grant 2019014.

ABSTRACT The Pulse-Pre-Pump Brillouin Optical Time Domain Analysis (PPP-BOTDA) based distributed fiber optic sensing (DFOS) technique has a unique advantage of achieving full-distributed structural strain with cm-order spatial resolution, which is ideal for fine stress monitoring of the pile foundation. The high spatial resolution helped to detect local changes and defects while inevitably led to noisy data meanwhile, especially a certain part of anomalous sensing data. Therefore, a robust algorithm of random sampling consistency (RANSAC) was employed to extract and process the DFOS data. In a field static load test, the variation of strain along a precast pile was measured with PPP-BOTDA interrogator. The axial force and frictional resistance were calculated based on the RANSAC processed strain data. The pile-soil interface properties were estimated as well. It shows the feasibility and good performance of PPP-BOTDA in the measurement of precast piles stress test. The RANSAC proves to be an effective method for processing DFOS data with a certain number of outliers. This work presents a valuable reference for DFOS based pile stress test and data analysis which will promote its application in other related structural health monitoring purpose.

INDEX TERMS Distributed fiber optic sensing (DFOS), precast pile, pulse-pre-pump Brillouin optical time domain analysis (PPP-BOTDA), random sampling consistency (RANSAC), shaft friction monitoring.

I. INTRODUCTION

In the last two decades, the distributed fiber optic sensing (DFOS) technologies have received great attention, due to one of its most prominent advantages over conventional sensing technologies, that is the capability of continuous strain measurements within dozens of miles [1], [2]. By using this technology, more than thousands of sensing points along a fiber can be monitored simultaneously. Compared with traditional point measurement method, DFOS technologies can avoid detection omissions, obtain more information and reveal more details about the deformation distribution of the structures. The DFOS based monitoring results are undoubtedly more reliable.

Brillouin-based DFOS is one of the most applicable approaches which have been found a number of uses in civil engineering [3]–[7]. One of the most successful applications that reported is the stress monitoring of pile foundation [8]–[10]. The distributed strain results provide a new insight into the characteristics of pile–soil interaction and the load transfer mechanisms [11], [12]. The Pulse-Pre-Pump Brillouin Optical Time Domain Analysis (PPP-BOTDA) as a newly developed DFOS technology improves the spatial resolution to cm order, greatly increasing the sensing performance of DFOS for structural health monitoring (SHM) [13], [14].

Considering the harsh environments of civil engineering and other uncertain factors in field applications, it is difficult to guarantee the high installation quality of distributed optical fiber sensors at each point. Strain data of piles obtained by DFOS devices contain high noises, which will inevitably increase the difficulty of interpreting the measured result. A few data processing methods, such as polynomial fitting method [15], [16], Savitzky-Golay filtering [17], [18], moving averaging method, FFT filtering and wavelet analysis [19]–[21] have been adopted to process the DFOS signals. These common data processing methods can effectively reduce the randomness error in the measurement data. However, the data processing results are usually unsatisfactory

The associate editor coordinating the review of this manuscript and approving it for publication was Zhixiong Peter Li.

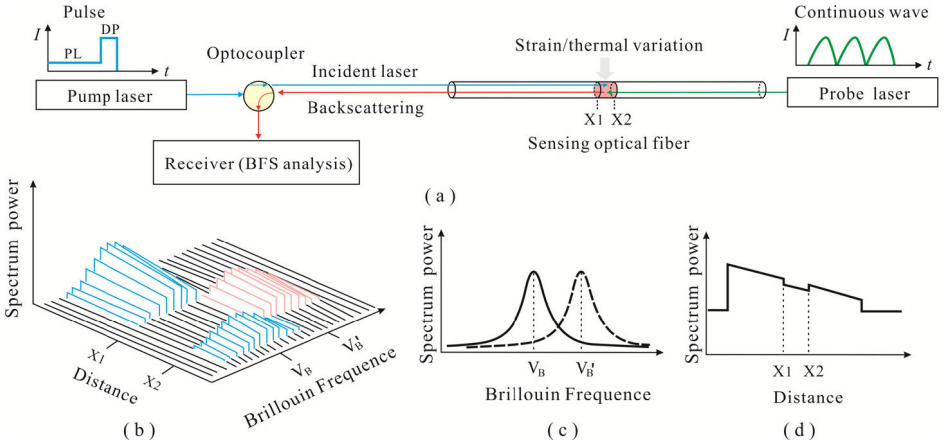

FIGURE 1. Principle of PPP-BOTDA.

if a high percentage of outliers (anomalous data) appear, especially when these outliers are distributed centrally in space with certain regularity.

Fischler and Bolles propose the idea of a random sampling consistency algorithm (RANSAC, RANdom SAmple Consensus) which is particularly suitable for handling data that contain outliers [22]. The RANSAC algorithm and its improved versions are now well applied in the field of computer vision processing area, proved to give a robust model results even when data contain high rates of outliers [23]. In this paper, the PPP-BOTDA based DFOS technology was used to obtain a precast pile strain data in the static load test. M-SAC (M-estimator SAmple Consensus) algorithm [24], an improved version of the RANSAC, was used to process the DFOS data to improve the reliability of the pile stress parameter estimation. It will help make a better use of PPP-BOTDA as well as other DFOS technology in the pile foundation test.

II. PRINCIPLE OF DFOS BASED PILE TESTING

A. PPP-BOTDA SENSING TECHNOLOGY

The well-known BOTDA is one of the most popular DFOS techniques. As shows in Figure 1, the pump pulse light launches at one end of the optical fiber and generates backward Brillouin gain. Whereas the probe light of continuous wave launches at the opposite end and propagates in the opposite direction, which interacts (amplifies) with the pump pulse light to create stimulated Brillouin scattering (SBS) light. The SBS light is associated with the Brillouin frequency shift (BFS) $\nu_B(\varepsilon, T)$. There is a linear relationship between $\nu_B(\varepsilon, T)$ and the strain ε, temperature T in the fiber optic sensor, which can be expressed as:

$$\nu_B(\varepsilon, T) = \nu_B(0, T_0) + C_1\varepsilon + C_2(T - T_0) \quad (1)$$

where $\nu_B(0, T_0)$ is the BFS at temperature T_0 with zero strain ε, C_1 is the strain coefficient, C_2 is the temperature coefficient.

PPP-BOTDA developed a pre-pump technique to improve the spatial resolution. The pump laser includes two types of pulses that, pre-pump laser (PL) to fully stimulate phonons while detecting pump (DP) to detect SBS. It can improve the spatial resolution of traditional BTODA from m to cm level. More details about the fundamentals of the PPP-BOTDA technology can be found in [13], [25].

In this study, the PPP-BOTDA based device used in this paper is the type NBX-6050A interrogator from Neubrex Co. Ltd Japan, which has the highest spatial resolution of 5cm and 1cm sampling spacing.

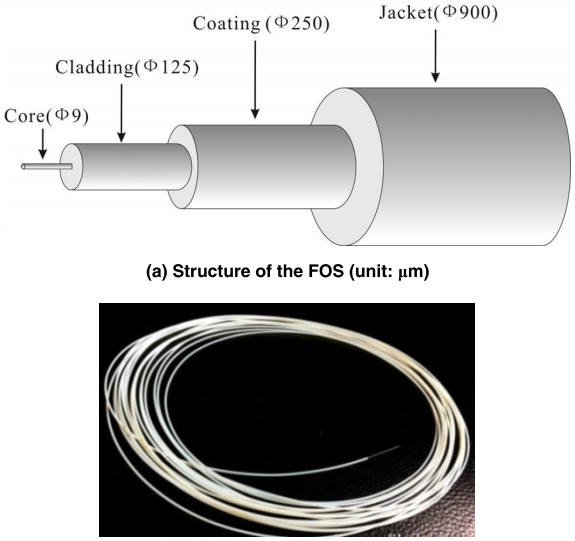

(a) Structure of the FOS (unit: μm)

(b) Photo of the FOS

FIGURE 2. Structure and photo of the distributed FOS.

B. DISTRIBUTED FIBER OPTIC SENSORS

The 0.9mm tight-buffered standard silicon fiber optic sensor (FOS) used in the test was produced by Suzhou Nanzee Sensing Co. Ltd, China. It is a common single-mode fiber (SMF) that has been widely used both in communication and sensing. As Figure 2 shows, the FOS consists of silicon core, cladding, coating and jacket from the inside out. The 325μm

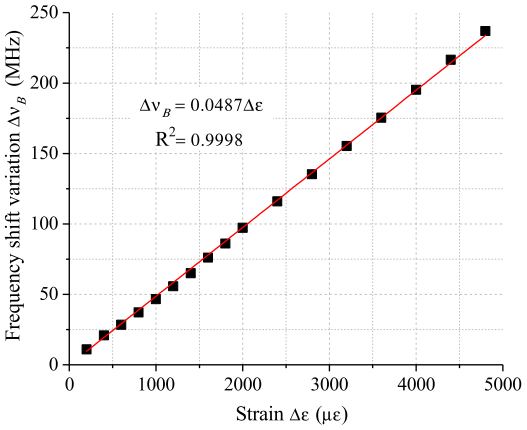

FIGURE 3. Relationship between BFS variation and optical fiber strain.

thick nylon jacket help increase mechanical strength of FOS. Its average Young's modulus was around 3GPa [26], [27].

The strain sensitivity coefficient C_1 in Eq. (1) was calibrated using a tensile tester and the results are shown in Figure 3. It shows an excellent linear relationship between BFS variation and optical fiber strain change at room temperature (22°C). The strain coefficient C_1 is 0.0487MHz/$\mu\varepsilon$. Since the change of the soil temperature is small during limited test time (around 30 hours) in the field static loading test [8], [28], the temperature effect was considered as an error term.

C. CALCULATION OF PILE STRESS WITH OPTICAL FIBER STRAIN

The derivation of pile axial strain $\varepsilon_{axial}(z)$ at depth z is done by averaging the strain $\varepsilon_A(z)$ and $\varepsilon_B(z)$ of two symmetric sensing fibers along the shaft to eliminate any bending effect of the pile.

$$\varepsilon_{\text{axial}}(z) = \frac{\varepsilon_A(z) + \varepsilon_B(z)}{2} \tag{2}$$

The relative displacement of pile-to-soil $S(z)$ at different pile depth z can be calculated as

$$S(z) = S(0) + \int_0^z \varepsilon_{axial}(z)dz \tag{3}$$

$S(0)$ is the settlement displacement measured at the pile head. The axial force $Q(z)$ at different pile depth z is expressed as

$$Q(z) = -\varepsilon_{axial}(z) \cdot E_c \cdot A \tag{4}$$

The elastic modulus E_c is obtained by inverse calculation, using the ratio of pile load to the pile head strain and assuming that E_c of the whole pile body is consistent. Then the pile tip resistance q_t and shaft friction resistance $q_s(z)$ can be determined as

$$q_t = \frac{Q(L)}{A} \tag{5}$$

$$q_s(z) = -\frac{1}{2\pi R}\frac{dQ(z)}{dz} \tag{6}$$

A is the pile cross-sectional area. L is the pile length. R is the external semidiameter of the pile.

In the design and evaluation of the actual pile foundation, people are generally concerned about the overall performance of the friction resistance of different soil layers that distributed over a certain range of depth. Based on Eq. (3) and Eq. (6), the average friction resistance $\overline{q_s(i)}$ and pile-to-soil relative displacement $\overline{S(i)}$ of the i^{th} soil layer can be determined as

$$\overline{q_s(i)} = -\frac{1}{2\pi R}\frac{Q(z_{top}(i)) - Q(z_{bottom}(i))}{z_{bottom}(i) - z_{top}(i)} \tag{7}$$

$$\overline{S(i)} = \frac{\int_{z_{bottom}(i)}^{z_{top}(i)} S(z)dz}{z_{bottom}(i) - z_{top}(i)} \tag{8}$$

where $z_{bottom}(i)$ and $z_{top}(i)$ are the depths of the bottom and top of the i^{th} soil layer respectively.

III. RANSAC BASED DFOS DATA PROCESSING

A. PRINCIPLE OF RANSAC ALGORITHM

RANSAC is an indeterminate algorithm that, with a certain number of iterations, ensures that at least one set of random samples without outliers can be selected with a certain confidence probability P. The specific process is as follows:

1. First a random sample set of data points d from the total observations D is selected, assuming that they are the data points of inliers (non-anomalous data). Suppose the data fit a parametric model, and the parameter can be determined with the inliers.

2. Evaluate all the other data with the model established in 1 based on a certain criteria. When the data meets this criterion, it is considered to be an inlier and expand the set of inliers.

3. If a sufficient number of data points are classified as hypothetical inliers, then the estimated model is reasonable enough.

The above entire process is regarded as once iteration and should be repeated for a certain number of times, each time resulting in a model with two outcomes: update the current data set of inliers as the optimal one if the number of inliers is larger than that of the last iteration; else, the model is discarded. In this way, an optimal set of inliers is determined after a finite number of iterations, based on which a model can be established. This model will eliminate the effect of outliers with a certain probability P.

B. DETERMINATION OF THE NUMBER OF ITERATIONS

Two key points needs to be specified here. The first one concerns the determination of the number of iterations and the reasonableness of the inliers assumption. w is the probability of inliers when select a sample data point randomly.

$$w = \frac{n_{\text{inliers}}}{n_{\text{inliers}} + n_{\text{outliers}}} \tag{9}$$

where n_{inliers} is the number of inliers; n_{outliers} is the number of outliers.

In general, we don't know the exact value of w beforehand, but can give some robust values. For example, suppose that the mathematical model solved by the RANSAC algorithm requires m points. The value of m is specifically determined by the problem being solved. When polynomial model is selected, m can be determined as the polynomial number plus one. Set the initial value of n_{inliers} equals to m, and w can be determined through Eq. (9).

w^m is the probability that all m data point are inliers, $1 - w^m$ is the probability that at least one of m points belongs to outliers. Then

$$1 - P = (1 - w^m)^k \tag{10}$$

where k is the number of iterations, and

$$k = \frac{\log(1 - P)}{\log(1 - w^m)} \tag{11}$$

With the progress of iterations, the number of estimated inliers expands. Correspondingly, the number of iterations that need to be satisfied to reach the same level of confidence decreases. Therefore, the algorithm can achieve fast convergence.

C. CRITERIA TO EXPAND THE SET OF INLIERS

The second is the criteria to expand the set of inliers mentioned in 2, which is actually called the minimization cost function J.

$$J = \sum_{d \in D} L(E(d; S)) \tag{12}$$

where L is loss function, E is the error function, which is defined as the Euclidean distance between the datum and the fitted model. S is the model parameter determined with the random sampling set d. Since the classical RANSAC algorithm pursues the number maximization of the inliers, the corresponding loss function L_R is:

$$L_R(e) = \begin{cases} 0 & e^2 \le t^2 \\ 1 & e^2 > t^2 \end{cases} \tag{13}$$

where e is the error value and t is the error threshold used to distinguish the inliers point from the outliers. Obviously, the loss function is entirely determined by the number of outliers. Thus, the algorithm is very sensitive to t. The M estimation sampling consistency algorithm (M-SAC) is an improved version of the RANSAC algorithm, which uses the bounded loss function L_M to alleviate this problem effectively. L_M takes accounts of effect of the inliers as well as the outliers.

$$L_M(e) = \begin{cases} \dfrac{e^2}{t^2} & e^2 \le t^2 \\ 1 & e^2 > t^2 \end{cases} \tag{14}$$

During the process of iteration, if the current cost function is smaller than the previous one, the current set of inliers is used to update the optimal one until the number of iterations reaches the set of maximum sampling times. For the error threshold t, it can be roughly determined by indoor tests.

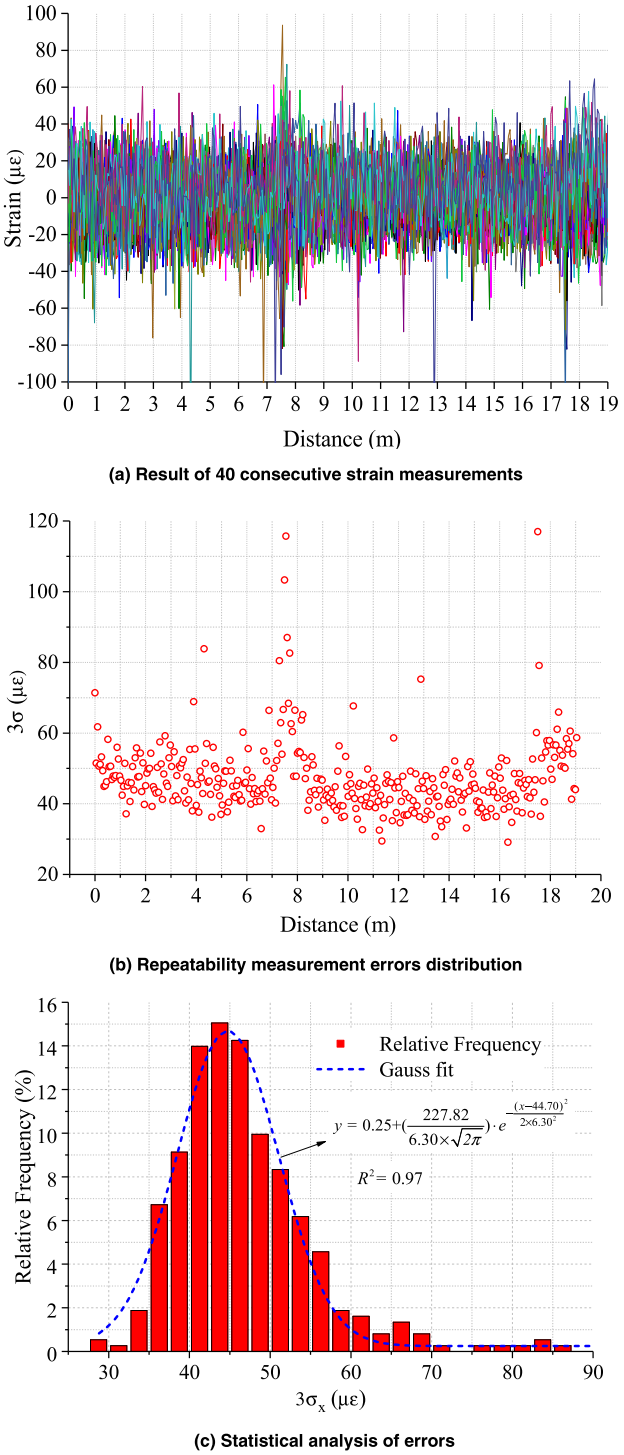

FIGURE 4. Measurement error of FOS.

Figure 4a shows the results of 40 repetitive PPP-BOTDA FOS tests. Repeatability error 3σ of FOS measurement is essentially similar at different locations except for a few segments (Figure 4b). Figure 4c is the frequency histogram of repeatability error values at different positions ($3\sigma_x$), and 99.7% confidence interval for repeatability error is $64\mu\varepsilon$ ($3\sigma_{3\sigma_x}$). Taking into account of the temperature-induced fluctuations (around $10\mu\varepsilon$) [28] and other additional factors in the actual

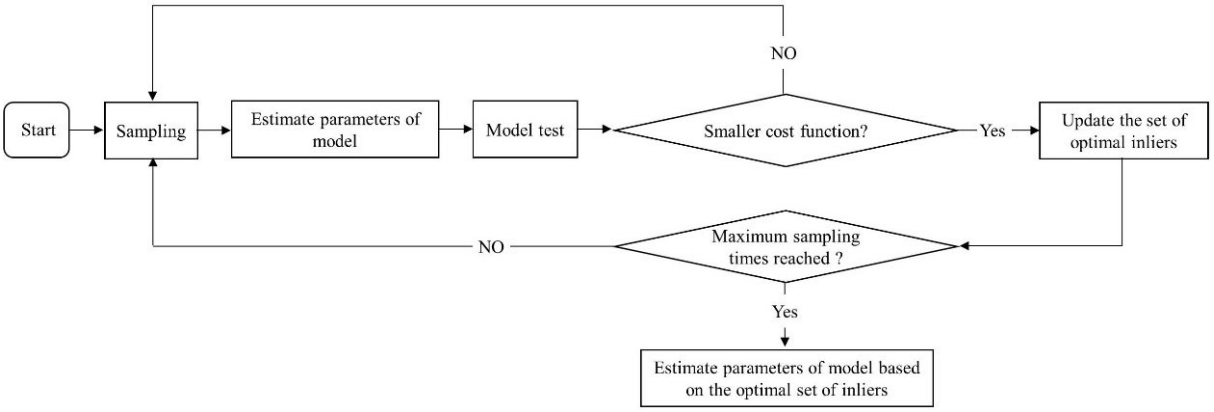

FIGURE 5. M-SAC algorithm flow-chart.

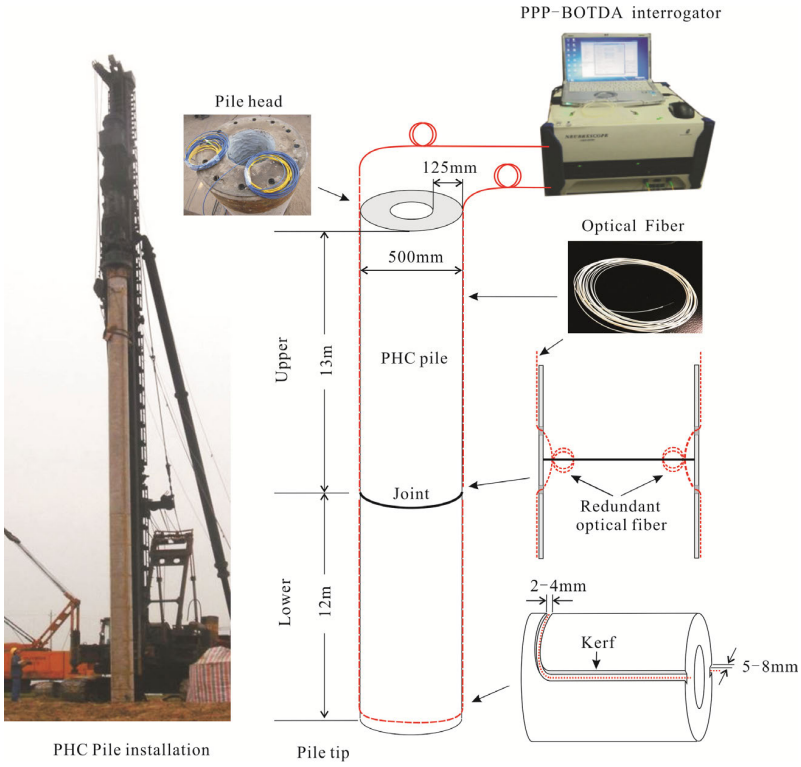

FIGURE 6. Layout of sensing optical fiber in the PHC pile.

test of engineering pile, the suggested value of parameter t was set to $80\mu\varepsilon$ in this paper.

Figure 5 shows the flow chart of M-SAC algorithm. The model is optimized by repeated random sampling, and the final model parameters are calculated from the optimal set of internal points.

IV. APPLICATION IN THE FIELD TEST

A. TEST SITE AND PILE CONDITIONS

A pile foundation was designed for a new hydropower plant. The pre-tensioned spun high strength concrete (PHC) precast piles with external diameter of 500mm and wall thickness of 125mm were used. The pile in this static loading test consists of two sections. The upper pile was 13m in length and 12m for the lower one. The concrete grade of the pile is C80. Details about the soil layers that were penetrated by the precast piles at the construction site are listed in Table 1.

B. LAYOUT OF SENSING OPTICAL FIBER

After several experiments, an effective method to embed the optical fibers into the PHC pile was employed in this project. The procedures for implementing slot embedding are presented as follows (Figure 6):

1) SLOTTING AND EMBEDDING

Along a designed line, two 3mm × 5mm (width × depth) kerfs were slotted and cleaned on the surface side of the pile. The sensing fibers were then embedded symmetrically into the slots along the lateral sides of the PHC pile.

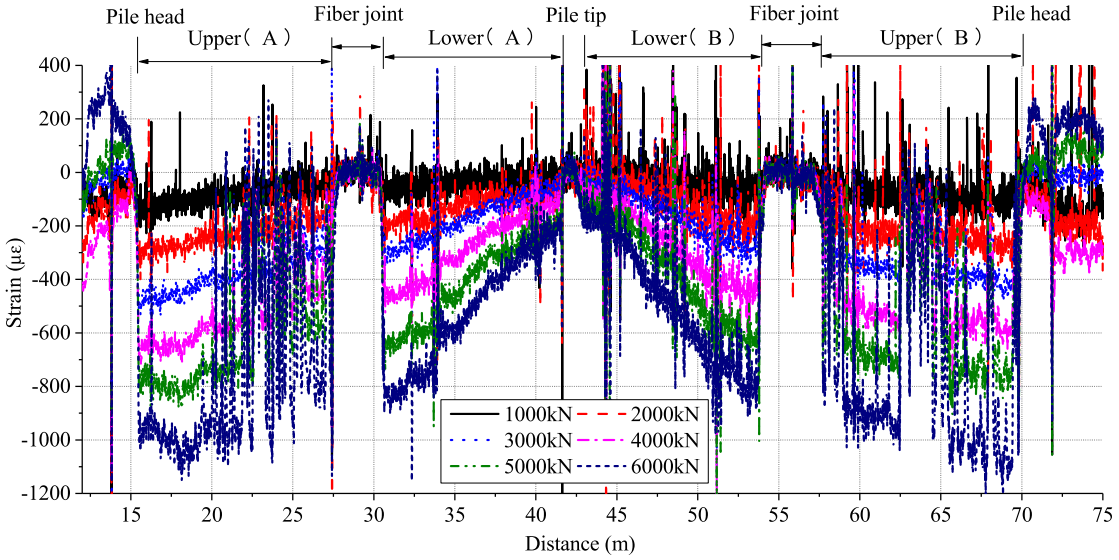

FIGURE 7. The measured strain curves of the sensing fiber under different loadings.

TABLE 1. Distribution of soil layers and their burial depths.

Soil layer number	Soil type	Burial Depth (m)	Mechanical parameters of the soil	
			Cohesion c (kPa)	Internal friction angle φ (°)
(1)	Fine sand	0-8.8	0	20.15
(2)	Silt	8.8-13.2	21.65	11.03
(3)	Medium sand	13.2-16.5	0	25.14
(4)	Silt	16.5-20.3	17.00	11.66
(5)	Medium sand	20.3-25	0	25.42

2) SEALING

The slots were filled with high strength epoxy resin adhesive, so as to bond the fibers to the pile surface.

3) JOINTING

In this project, it is inevitable for the jointing of two sections of pile with embedded fibers. Instantaneous strain between two sections may be great during the process of pile installation. To reduce the possibility of FOS failure, the redundant optical fibers of two sections at the joint point were fused and put inside the pile.

V. TEST RESULTS AND ANALYSES

A. STRAIN DISTRIBUTION OF PILE

The strain distribution and changes of the pile under each loading were obtained as illustrated in Figure 7. It shows a relatively symmetrical profile which represents the loop setup of optical strain sensing fiber. The data of sensing optical fiber from about 15.45m to 41.68m correspond to one side of the pile (side A).

The data that from 42.65m to 69.7m correspond to the other side (side B). There are two distinct regions on each side which represent the two jointing piles (upper (A), lower (A) and upper (B), lower (B)). The data of fiber joint represent the redundancy of optical fiber that lies between the upper and the lower pile.

B. DATA PROCESSING

According to the measured DFOS data in Figure 7, the compression strain of pile increases progressively with the applied loads. The monitored data of both side (A) and side (B) were picked out as the strain value of the whole pile body (Figure 8a and Figure 8b). For side (A), the effective strain data of the upper pile are from 15.45m to 27.45m which correspond to 0.5m-12.5m, and data from 30.58m to 41.68m are for the lower which correspond to 13.35m-24.45m. For side (B), raw strain data of the upper pile are from 69.70m to 57.70m, and the lower are from 53.75m to 42.65m.

We take the average measured strain of the opposite pile side A and side B as the axial strain of the pile body to eliminate any bending effect based on Eq. (2). Then the distribution axial strain curves of the whole pile foundation are obtained as shown in Figure 8c.

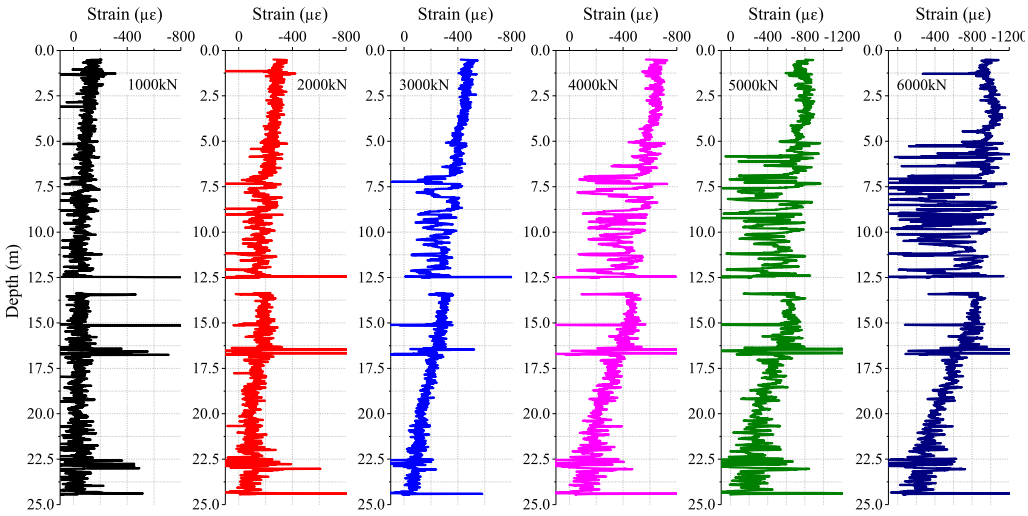

(a) Pile Strain profile for side (A)

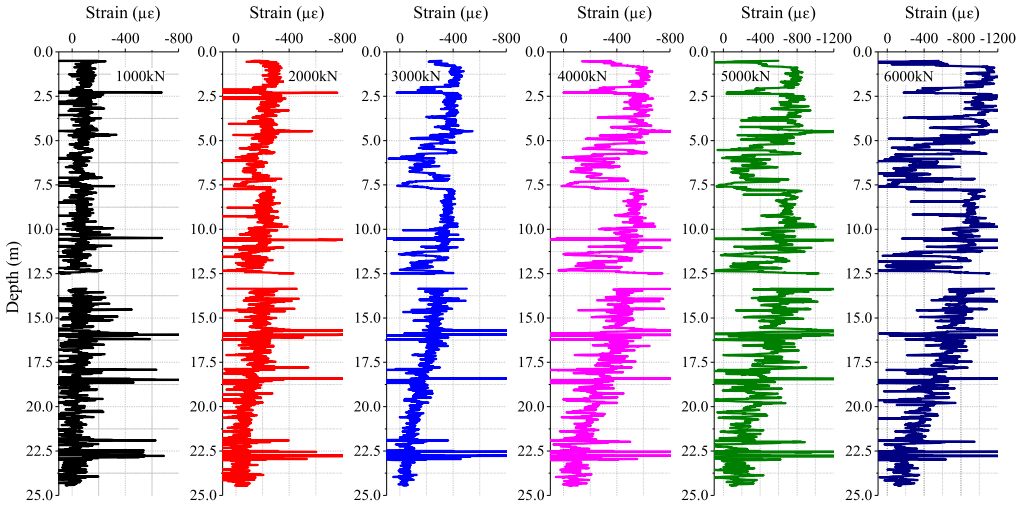

(b) Pile Strain profile for side (B)

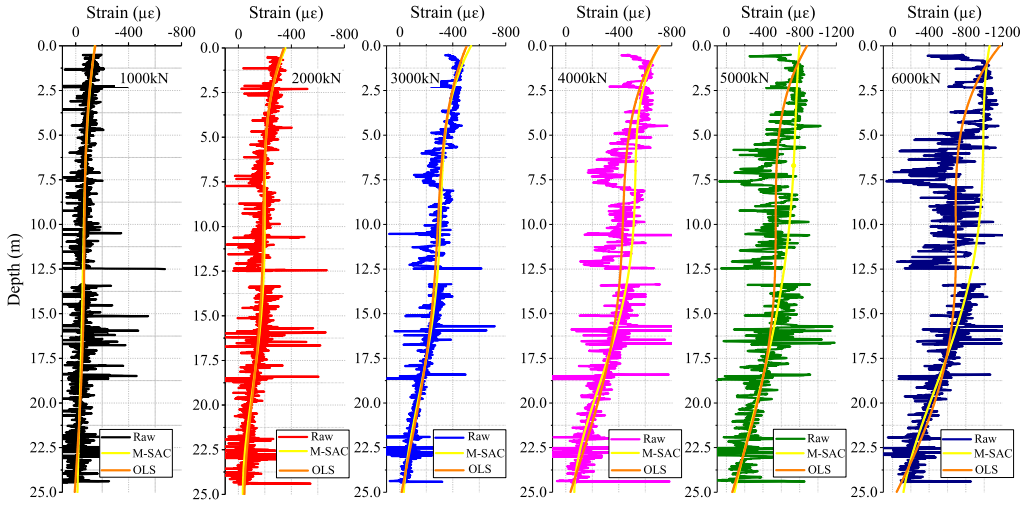

(c) Pre and post of RANSAC and OLS processing of pile strain profile for the average of side (A) and side (B)

FIGURE 8. PPP-BOTDA based measurement of pile strain profiles.

According to the theoretical load transmission characteristics of PHC pile, the axial strain should vary in such a trend that the strain decreases gradually with the depth of PHC pile. However, it was found that obviously anomalous axial strain data at some local positions of the upper pile body (5-8m, 11-12.5m) could be spotted when the applied static load exceeded 3000kN. The measured strain values at these positions are inconsistent with the pile theory and instead the values vary from sharp decrease to increase at certain locations, and both the number and magnitude of the anomalous data increased with the applied static loads upon PHC pile. Therefore, the ideal fitting model of pile strain data should avoid these outliers to a greater extent to reduce their effect on the model as a matter of experience.

Then, the M-SAC algorithm that described in section 3 was used to process the DFOS data with obvious outliers. Here we selected 4^{th} order polynomial function as the predictive model, and set the error threshold t to $80\mu\varepsilon$. Afterwards, the data were also processed by traditional polynomial fitting algorithm based on the ordinary least square (OLS) method for comparison [15]. The final processed strain profiles (yellow lines for M-SAC algorithm and orange lines for OLS) of the whole pile are shown in Figure 8c. It shows that the results of the two algorithms are basically the same when the applied static load is relatively small since the observed outliers are subtler. When the applied static load exceeds 3000kN, the results drawn from the two algorithms diverge as the outliers increase. The M-SAC based algorithm has a good shielding effect upon the outliers, while the fitting curve processed by OLS algorithm is obviously affected by the outliers. The data model based on OLS algorithm treats the outliers as normal data, which leads to the sharp slope change at some locations of the curve. In terms of Eq. (4) and Eq. (6), friction resistance that is much higher than the empirical normal values will exist at some locations of soil layers, which is obviously unreasonable. In this sense, the M-SAC algorithm can better meet our expected effect in processing the data with a certain number of outliers (anomalous data).

C. LOAD TRANSFER MECHANISM

When the loading value was divided by the fitted strain at the pile head, the elastic modulus E_c used for the calculation of pile axial force could be determined. The distribution profile of axial force and shaft friction of pile under different loads can be calculated using the strain data based on Eq. (4) and Eq. (6), and the results are illustrated in Figure 9a and Figure 9b.

As Figure9c shows, when the load was smaller than 3000kN, the shaft friction resistance (SF) contributed by soil layer (1) is the largest. When the load increased, frictions began to mainly concentrate in the soil layers (3), (4) and (5) while decreased in soil layer (1). SF that soil layer (2) offered was relatively low all the time. Figure 10 shows the settlement recorded at the pile head under different loads and Figure11 is the vertical displacement curves $S(z)$ along the pile calculated based on Eq. (8).

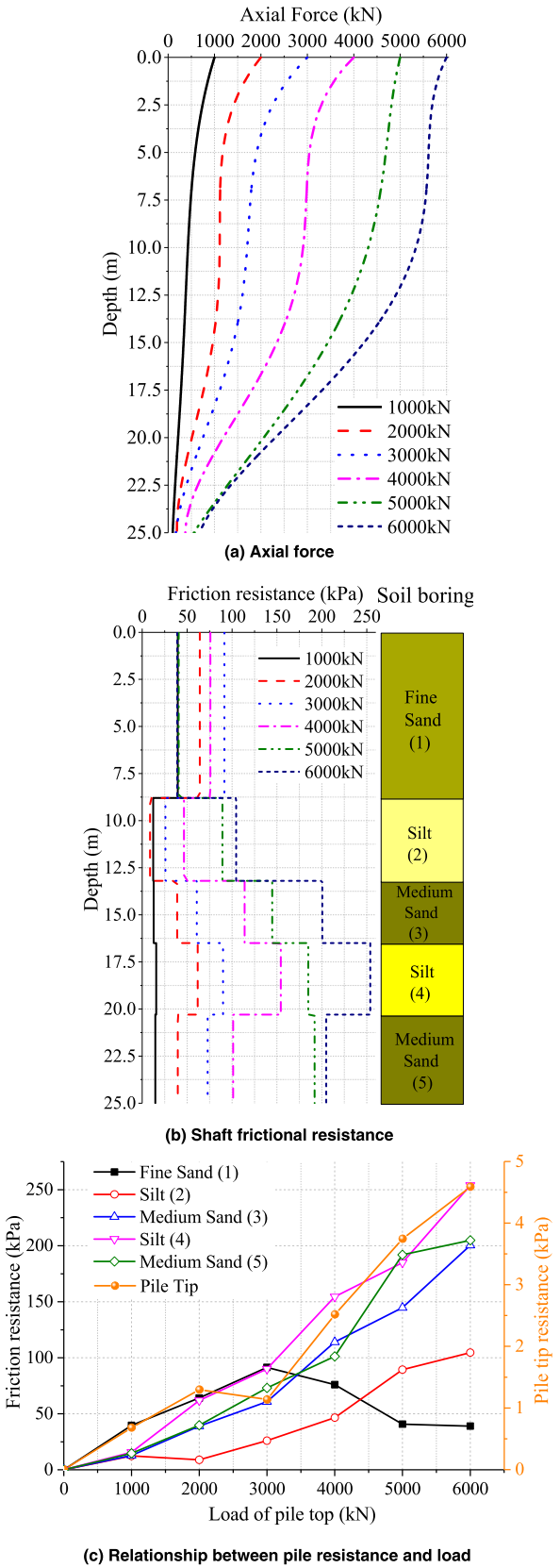

FIGURE 9. Profiles of pile stress.

Based on Eq. (5), (7) and (8), the evolution of pile tip and SF resistance with the local vertical displacement can be

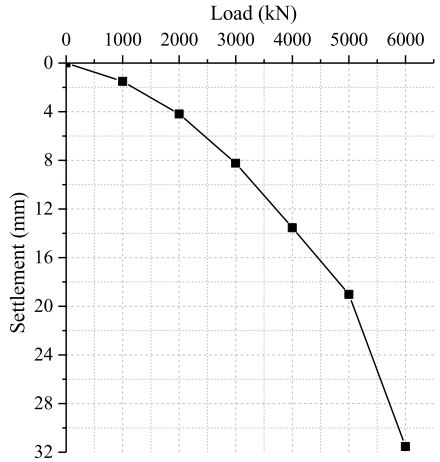

FIGURE 10. Load-settlement at the pile head.

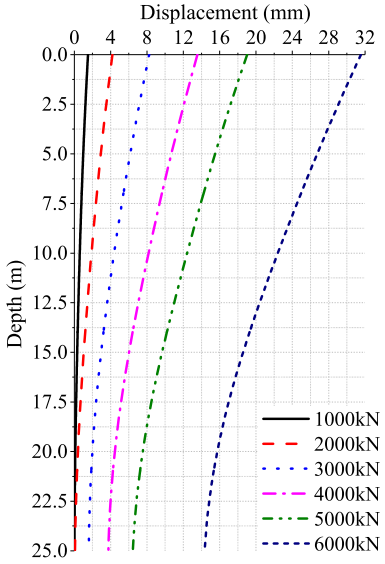

FIGURE 11. Displacement profile for different load steps.

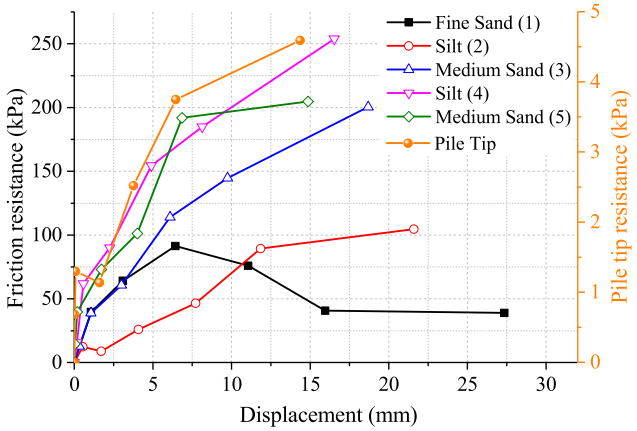

FIGURE 12. Load transfer curve for different soil layers.

calculated as Figure 12 displayed. Both the pile SF and tip resistance development curves show an initial stiffness that decreased with the displacement. SF of fine sand (1) exhibits strain-softening characteristics, Silt (2) and Medium sand (5) roughly reached a plateau, while Silt (4) and Medium sand (3) seems to have not reached the maximum yet.

VI. CONCLUSION

A novel full DFOS system based on PPP-BOTDA technique was employed to continuously measure the stress of a PHC pile in the field. The robust algorithm of RANSAC was used to process the monitored DFOS data of pile. Based on the above result, the main implications and conclusions can be summarized as bellow:

(1) The PPP-BOTDA-based precast pile test methodology is effective to obtain the pile strain distributions. However, some local anomalies were found in the FOS measured pile strain data and became more pronounced as the load increased.

(2) Calculation equations for axial force, shaft friction and tip resistance, the relative displacement of pile-to-soil with PPP-BOTDA measured strain data were deduced and presented. The robust algorithm of RANSAC based model can effectively eliminate the effect of anomalous data

(3) The mechanism of pile-soil interactions was analyzed based on the RANSAC processed DFOS data. The pile shaft friction mainly bears most part of the load and strain softening phenomenon appear in the first soil layer while the shaft friction resistance of soil layers in the deep and pile tip resistance did not yet reach the ultimate resistance when the maximum load is applied.

REFERENCES

[1] C.-Y. Hong, Y.-F. Zhang, G.-W. Li, M.-X. Zhang, and Z.-X. Liu, "Recent progress of using Brillouin distributed fiber optic sensors for geotechnical health monitoring," *Sens. Actuators A, Phys.*, vol. 258, pp. 131–145, May 2017.

[2] X. Bao and L. Chen, "Recent progress in distributed fiber optic sensors," *Sensors*, vol. 12, no. 7, pp. 8601–8639, Jun. 2012.

[3] W. R. Habel and K. Krebber, "Fiber-optic sensor applications in civil and geotechnical engineering," *Photon. Sensors*, vol. 1, no. 3, pp. 268–280, Sep. 2011.

[4] K. Soga and L. Luo, "Distributed fiber optics sensors for civil engineering infrastructure sensing," *J. Struct. Integrity Maintenance*, vol. 3, no. 1, pp. 1–21, Jan. 2018.

[5] A. Barrias, J. R. Casas, and S. Villalba, "A review of distributed optical fiber sensors for civil engineering applications," *Sensors*, vol. 16, p. 748, Oct. 2016.

[6] L. Schenato, "A review of distributed fibre optic sensors for geo-hydrological applications," *Appl. Sci.*, vol. 7, no. 9, p. 896, Sep. 2017.

[7] N. Nöther, "Distributed Brillouin sensing for geotechnical infrastructure: Capabilities and challenges," *Geotech. Eng. J. SEAGS AGSSEA*, vol. 50, no. 2, pp. 8–12, Jun. 2019.

[8] Y. Lu, B. Shi, G. Q. Wei, S. E. Chen, and D. Zhang, "Application of a distributed optical fiber sensing technique in monitoring the stress of precast piles," *Smart Mater. Struct.*, vol. 21, pp. 115011–115019, Sep. 2012.

[9] B. Liu, D. Zhang, and P. Xi, "Mechanical behaviors of SD and CFA piles using BOTDA-based fiber optic sensor system: A comparative field test study," *Measurement*, vol. 104, pp. 253–262, Jul. 2017.

[10] H. Mohamad, K. Soga, P. J. Bennett, R. J. Mair, and C. S. Lim, "Monitoring twin tunnel interaction using distributed optical fiber strain measurements," *J. Geotechnical Geoenvironmen. Eng.*, vol. 138, no. 8, pp. 957–967, Aug. 2012.

[11] S. Bersan, O. Bergamo, L. Palmieri, L. Schenato, and P. Simonini, "Distributed strain measurements in a CFA pile using high spatial resolution fibre optic sensors," *Eng. Struct.*, vol. 160, pp. 554–565, Apr. 2018.

[12] L. Pelecanos, K. Soga, M. Z. E. B. Elshafie, N. de Battista, C. Kechavarzi, C. Y. Gue, Y. Ouyang, and H.-J. Seo, "Distributed fiber optic sensing of axially loaded bored piles," *J. Geotechnical Geoenvironmental Eng.*, vol. 144, no. 3, Mar. 2018, Art. no. 04017122.

[13] H. Zhang and Z. Wu, "Performance evaluation of PPP-BOTDA-Based distributed optical fiber sensors," *Int. J. Distrib. Sensor Netw.*, vol. 8, no. 12, Dec. 2012, Art. no. 414692.
[14] D. Meng, F. Ansari, and X. Feng, "Detection and monitoring of surface micro-cracks by PPP-BOTDA," *Appl. Opt.*, vol. 54, no. 16, p. 4972, May 2015.
[15] Y. Ding, P. Wang, and S. Yu, "A new method for deformation monitoring on H-pile in SMW based on BOTDA," *Measurement*, vol. 70, pp. 156–168, Jun. 2015.
[16] Z. Wu, B. Xu, K. Hayashi, and A. Machida, "Distributed optic fiber sensing for a full-scale PC girder strengthened with prestressed PBO sheets," *Eng. Struct.*, vol. 28, no. 7, pp. 1049–1059, Jun. 2006.
[17] H. Mohamad, K. Soga, A. Pellew, and P. J. Bennett, "Performance monitoring of a secant-piled wall using distributed fiber optic strain sensing," *J. Geotechn. Geoenvironmen. Eng.*, vol. 137, no. 12, pp. 1236–1243, Dec. 2011.
[18] H. Mohamad and B. Pin Tee, "Instrumented pile load testing with distributed optical fibre strain sensor," *Jurnal Teknologi*, vol. 77, no. 11, pp. 93–186, Nov. 2015.
[19] Y. Ding, B. Shi, and D. Zhang, "Data processing in BOTDR distributed strain measurement based on pattern recognition," *Optik*, vol. 121, no. 24, pp. 2234–2239, Dec. 2010.
[20] L. Gao, C. Han, Z. Xu, Y. Jin, and J. Yan, "Experimental study on deformation monitoring of bored pile based on BOTDR," *Appl. Sci.*, vol. 9, no. 12, p. 2435, Jun. 2019.
[21] J. He, "Measurement accuracy improvement of Brillouin signal using wavelet denoising method," *Smart Struct. Mater., Nondestruct. Eval. Health Monitor.*, vol. 4, pp. 72930–72937, Apr. 2009.
[22] M. A. Fischler and R. Bolles, "Random sample consensus: A paradigm for model fitting with applications to image analysis and automated cartography," *Commun. ACM*, vol. 24, no. 6, pp. 381–395, 1981.
[23] Y. Li and N. R. Gans, "Predictive RANSAC: Effective model fitting and tracking approach under heavy noise and outliers," *Comput. Vis. Image Understand.*, vol. 161, pp. 99–113, Aug. 2017.
[24] P. H. S. Torr and A. Zisserman, "MLESAC: A new robust estimator with application to estimating image geometry," *Comput. Vis. Image Understand.*, vol. 78, no. 1, pp. 138–156, Apr. 2000.
[25] Y. Bao, "Novel applications of pulse pre-pump Brillouin optical time domain analysis for behavior evaluation of structures under thermal and mechanical loading," Ph.D. dissertation, Civil, Archit. Environ. Eng., Missouri Univ. Sci. Techn., Rolla, MO, USA, 2017.
[26] C.-C. Zhang, H.-H. Zhu, B. Shi, and J.-K. She, "Interfacial characterization of soil-embedded optical fiber for ground deformation measurement," *Smart Mater. Struct.*, vol. 23, no. 9, Sep. 2014, Art. no. 095022.
[27] B.-J. Wang, K. Li, B. Shi, and G.-Q. Wei, "Test on application of distributed fiber optic sensing technique into soil slope monitoring," *Landslides*, vol. 6, no. 1, pp. 61–68, Mar. 2009.
[28] C. D. Piao, B. Shi, and L. Gao, "Characteristics and application of botdr in distributed detection of pile foundation," *Adv. Mater. Res.*, vol. 163, pp. 163–167, Mar. 2010.

YIJIE SUN received the Ph.D. degree in geological engineering from Nanjing University, China, in 2015. He is currently an Assistant Professor with the College of Transportation Science and Engineering, Nanjing Tech University, China. His research interests include distributed fiber optic sensing technology-based geological body and geotechnical engineering structure health monitoring, data processing methods, and geological hazard assessment.

XUAN LI was born in Yangquan, China, in 1994. She received the bachelor's degree from the College of Transportation Science and Engineering, Nanjing Tech University, where she is currently pursuing the master's degree in geological engineering with the College of Transportation Science and Engineering. Her research interests include surrounding rock classification and shield construction.

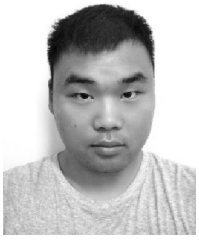

CUN REN was born in Anhui, China, in 1996. He received the bachelor's degree in exploration technology and engineering from Nanjing Tech University, in 2019, where he is currently pursuing the master's degree in geological engineering. His research interests include in-situ tests and optical fiber sensing technology.

HONGZHONG XU received the Ph.D. degree in hydraulic structural engineering from Hohai University, China, in 2001. He is currently a Professor with the College of Transportation Science and Engineering, Nanjing Tech University, China. His research interests include distributed fiber optic sensing technology-based geotechnical engineering structure health monitoring, building foundation excavations, and reinforced slope engineering.

AIMIN HAN received the master's degree in engineering geology from Nanjing University, China, in 1992. He is currently a Professor with the College of Transportation Science and Engineering, Nanjing Tech University, China. His research interests include the engineering characteristics of regional soils in China, building foundation excavations, slope, and tunnel engineering.